D'Mello *et al. Integrating Materials and Manufacturing Innovation* (2015) 4:7
DOI 10.1186/s40192-015-0035-y

Integrating Materials and Manufacturing Innovation
a SpringerOpen Journal

RESEARCH ARTICLE Open Access

Effect of the curing process on the transverse tensile strength of fiber-reinforced polymer matrix lamina using micromechanics computations

Royan J D'Mello[1,2], Marianna Maiarù[1,2] and Anthony M Waas[1,2*]

*Correspondence:
awaas@aa.washington.edu
[1]Composite Structures Laboratory, Department of Aerospace Engineering, University of Michigan, 1320 Beal Avenue, Ann Arbor, MI 48109-2140, USA
[2]William E. Boeing Department of Aeronautics and Astronautics, University of Washington, Seattle, WA 98195-2400, USA

Abstract

The effect of the curing process on the mechanical response of fiber-reinforced polymer matrix composites is studied using a computational model. Computations are performed using the finite element (FE) method at the microscale where representative volume elements (RVEs) are analyzed with periodic boundary conditions (PBCs). The commercially available finite element (FE) package ABAQUS is used as the solver, supplemented by user-written subroutines. The transition from a continuum to damage/failure is effected by using the Bažant-Oh crack band model, which preserves mesh objectivity. Results are presented for a hexagonally packed RVE whose matrix portion is first subjected to curing and subsequently to mechanical loading. The effect of the fiber packing randomness on the microstructure is analyzed by considering multi-fiber RVEs where fiber volume fraction is held constant but with random packing of fibers. The possibility of failure is accommodated throughout the analysis—failure can take place during the curing process prior to the application of in-service mechanical loads. The analysis shows the differences in both the cured RVE strength and stiffness, when cure-induced damage has and has not been taken into account.

Keywords: Curing; Stress evolution; Periodic boundary condition; Crack band model

Background

Fiber-reinforced polymer matrix composites (FRPCs) are high-strength and lightweight advanced materials widely used in the aerospace and automotive industries. Since FRPCs are manufactured by curing the matrix that surrounds the interspersed fibers, good understanding of the matrix state during the curing process is necessary to have sufficient control over the quality of the cured product. The mechanical properties of the matrix during curing can be altered by the presence of fibers and also by details of the curing cycle. The curing matrix undergoes shrinkage due to chemical processes, which gives rise to self-equilibrating internal stresses. Plepys and Farris [1] and Plepys et al. [2] have used finite element calculations using incremental elasticity to show tensile residual stress buildup of up to 28 MPa post cure in a three-dimensionally constrained Epon 828 epoxy resin. Merzlyakov et al. [3] reported the development of tensile stresses in a constrained thermosetting resin system undergoing cure and also quantified the variation of these

tensile stresses during subsequent thermal cycling. Depending on the constituent chemistry of the matrix, the thermal cycle prescribed, and the fracture and strength properties of a curing matrix, a fiber-reinforced composite can and may undergo damage and cracking in the matrix during the cure cycle. Chekanov et al. [4] have reported various types of defects that may form in a constrained epoxy resin system undergoing curing. Rabearison et al. [5] studied the curing of a thick epoxy tube using a finite element model and concluded that high stress gradients developed during differential curing can cause cracking. Therefore, the state of the matrix within a cured FRPC structure exhibits *in situ* matrix properties, which are effective properties of the matrix that take into account imperfections caused in the matrix due to the cure process, including the presence of residual stresses. That is, the *in situ* matrix properties, where the matrix is treated as a 'new' material with a reference configuration that corresponds to the post-cured state, deviate from idealized or 'virgin' matrix properties of the bulk matrix. The *in situ* matrix properties can be extracted from an inverse analysis [6] through the uniaxial tensile response of a $\pm 45^\circ$ laminate, and this is convenient in engineering analysis of cured composites. Song and Waas [7] have shown that the use of bulk matrix properties in numerical predictions of compression response of a 2D triaxially braided composite RVE can lead to erroneous results - the computed compressive strength being noticeably higher than the experimentally measured strength. They observed that the tow kinking failure mode, which controls the compression strength was found to be sensitive to the nonlinear shear response of the matrix. Cure shrinkage in the matrix surrounded by randomly dispersed fibers can also influence the final shape of the structure [8]. Therefore, it is necessary to have good knowledge of the influence of the cure cycle on the subsequent mechanical response of the laminate. For a particular fiber-matrix laminate system, the optimal cure cycle can be identified such that the cured product has the highest strength and stiffness. Efforts to optimize various aspects of the cure cycle for mitigating the residual stresses generated during cure can be found in the studies of Li et al. [9], Gopal et al. [10], and White and Hahn [11].

In the present investigation, the effects of the cure cycle on possible damage accumulation during cure and subsequent in-service performance at the microstructural level are studied. A hexagonally packed representative volume element (RVE) having a total of two fibers (one full center fiber and quarter fibers at four corners) with different volume fractions, and a randomly packed RVE having multiple fibers are studied. First, the influence of fiber volume fraction on the strength of the cured RVE using the hexagonally packed RVE with two fibers is studied. Next, the effect of the randomness of the packing for RVEs having fixed volume fraction is investigated. For illustrating the findings of this study, the strength investigated is the transverse tensile strength (S_{22}^{+}), which is obtained by mechanically loading each of the virtually cured RVEs along the transverse direction under tension. Then, the initial slope and peak stress value of the nominal stress-strain response are the transverse stiffness E_{22} and transverse tensile strength S_{22}^{+}, respectively. For low to moderate fiber volume fractions, the transverse stiffness is controlled by matrix stiffness (see [12]). The transverse tensile strength associated with *transverse matrix cracking* is controlled by a combination of factors such as matrix tensile strength, matrix fracture toughness, fiber packing, and adhesion strength between fibers and the matrix. Hence, it is expected that both E_{22} and S_{22}^{+} are influenced by the details of the cure process.

Methods

Cure process

The curing process of a thermoset polymer can be divided into two parts: The first part consists of the chemical reaction, heat generation, and conduction. The second is the generation of self-equilibrating stresses and development of the structural integrity via the evolution of matrix stiffness. The stress generation has been modeled by Mei [13], Mei et al. [14], and Heinrich et al. [15]. The degree of cure (ϕ) of the matrix is defined as $\phi = H(t)/H_{\mathrm{r}}$, where $H(t)$ is the heat generated up to time t, and H_{r} is the total heat of reaction at the end of the cure cycle. Mathematically, the rate of cure $\left(\frac{d\phi}{dt}\right)$ can be expressed as,

$$\frac{d\phi}{dt} = f(T,\phi) \tag{1}$$

where $f(T,\phi) \geq 0$ is a function. The evolution of temperature (T) and degree of cure (ϕ) for the matrix material system is determined through a coupled system that considers the heat equation and an empirical curing law or can be supplied from the output of a simulation that takes into account a cure kinetics model. Kamal [16] has proposed a semi-empirical expression for the function $f(T,\phi)$ in terms of Arrhenius terms that depend on temperature

$$f(T,\phi) = \left[A_1 \exp\left(\frac{\Delta E_1}{TR}\right) + A_2 \exp\left(\frac{\Delta E_2}{TR}\right)\phi^m\right](1-\phi)^n \tag{2}$$

where T is temperature, R is the gas constant, and ΔE_1 and ΔE_2 are activation energies. The frequency-like constants A_1, A_2 and exponents m and n, in theory, have to be determined by fitting the above equation to the experimental data. However, due to the complexity of the function $f(T,\phi)$, a general closed formed solution to Equation 1 is elusive, and often times, this differential equation has to be solved using some numerical method. Assuming the form for $f(T,\phi)$ in Equation 2 by setting $m = A_2 = \Delta E_2 = 0, n = 1$ and under isothermal conditions, an explicit relation between the degree of cure and time can be found as a solution to the differential equation 1, which is

$$\phi(t) = 1 - \exp(-\lambda t) \tag{3}$$

where the Arrhenius parameter $\lambda = A_1 \exp\left(\frac{-\Delta E_1}{TR}\right)$. Cure data as a function of time for Epon 862/Epikure 9553 resin under isothermal conditions are chosen for the present work and are available in [15]. The constants obtained by curve fitting with experimental data at various temperatures are as follows: $A_1 = 3.62 \times 10^{11}\ \mathrm{s}^{-1}$ and $\Delta E_1 = 8.854 \times 10^4$ J.

During curing, the matrix heats up due to an exothermic chemical reaction and due to conduction from the heating source at the boundary. This process can be modeled using the equation

$$\rho c \frac{\partial T}{\partial t} = \frac{\partial}{\partial x_i}\left(\kappa(T,\phi)\frac{\partial T}{\partial x_i}\right) + \rho H_r \frac{\partial \phi}{\partial t} \tag{4}$$

where ρ is the mass density, c_p is the specific heat, and κ is the thermal conductivity. The evolution of self-equilibrating stresses $\sigma_{ij}(t)$ during curing is included in the analysis by using a model proposed by Heinrich et al. [15]:

$$\begin{aligned}\underline{\underline{\sigma}}(t) = \int_0^t \frac{d\phi}{ds}\underline{\underline{1}}\Big[K(s)tr\left(\underline{\underline{\varepsilon}}(t) - \underline{\underline{\varepsilon}}(s) + \underline{\underline{\varepsilon_c}}(s) - \underline{\underline{1}}\alpha(s)\Delta T(t,s)\right)\\ +\ 2\mu(s)\left(\underline{\underline{\varepsilon}}(t) - \underline{\underline{\varepsilon}}(s) + \underline{\underline{\varepsilon_c}}(s) - \underline{\underline{1}}\frac{1}{3}tr\{\underline{\underline{\varepsilon}}(t) - \underline{\underline{\varepsilon}}(s) + \underline{\underline{\varepsilon_c}}(s)\}\right)\Big] ds\\ +(1-\phi(t))K(0)tr(\underline{\underline{\varepsilon}}(t) - \underline{\underline{1}}\alpha(0)\Delta T(t))\underline{\underline{1}}\end{aligned} \tag{5}$$

where K, μ, α, and ε_c are the per-network bulk modulus, shear modulus, coefficient of thermal expansion, and cure shrinkage, respectively. The first term having the integral is the contribution to stress evolution due to the curing matrix, whereas the second term captures the contribution of the uncured liquid resin. The constants $K(0)$ and $\alpha(0)$ correspond to the bulk modulus and coefficient of thermal expansion of the liquid resin, respectively. The coefficient of thermal expansion $\alpha(\phi)$ of the curing matrix is assumed to have a constant value of 61×10^{-6} m/mK. As shown by Heinrich et al. [15], the per-network properties can be obtained from experimentally measured values of the plane wave modulus (M_{exp}) and shear modulus (μ_{exp}) for the curing matrix as

$$\begin{aligned}M(\phi) &= \frac{dM_{\text{exp}}}{d\phi} + K_{\text{exp}}(0)\\ \mu(\phi) &= \frac{d\mu_{\text{exp}}}{d\phi}\end{aligned} \tag{6}$$

The moduli values M_{exp} and μ_{exp} are measured as a function of time by concurrent Raman and Brillouin light scattering for the pure resin, that is, for a resin curing in the absence of fibers. These moduli are assumed to correspond to the virgin matrix as a function of degree of cure. The effect of the presence of fibers around the matrix on matrix degradation during cure will be demonstrated later in this paper. Once $M(\phi)$ and $\mu(\phi)$ are known, the per-network bulk modulus $K(\phi)$ can be obtained from the isotropic material relation $K = M - \frac{4}{3}\mu$. The per-network shrinkage strain $\varepsilon_c(\Phi)$ up to a certain degree of cure $\phi = \Phi$ is given by

$$\varepsilon_c = \frac{1}{3K(\Phi)}\left[\left(\varepsilon(\Phi) - (1-\Phi)\frac{d\varepsilon(\Phi)}{d\Phi}\right)K_{\text{exp}} - \frac{d\varepsilon(\Phi)}{d\Phi}\int_0^{\Phi} M(\phi)d\phi\right] \tag{7}$$

A gravimetric test method (see [17]) can be used to obtain shrinkage of all networks $\varepsilon(\Phi)$. A 2% per-network cure shrinkage has been chosen for the present investigation.

Damage during cure

During curing, the matrix gradually solidifies (stiffness increases) and simultaneously contracts (cure shrinkage) due to network formation. Residual stresses develop in the matrix owing to cure shrinkage and thermal strains. Depending on the magnitude of tensile stresses developed, the degree of cure (ϕ), and the rate of cure $\left(\frac{d\phi}{dt}\right)$, the material may crack locally during curing. A crack band model is used to simulate the possibility of tensile cracking during the curing of the matrix. The critical tensile stress for cracking typically increases with the degree of cure. If certain matrix regions crack locally, it would result in a reduction in the matrix stiffness in that local region along with some energy dissipated due to cracking. Such a reduction in local matrix stiffness can control the mechanical properties of the cured RVE. Two assumptions are enforced because the degree of cure and the coefficient of thermal expansion of a partially cured local volume of material with microcracks are unknown and physically this local volume does not represent a continuum in the strictest sense. First, if a certain local volume of material cracks,

it is assumed that no further curing can take place in that local volume. Second, it is assumed that if cracking occurs locally, the local cracked volume cannot expand or contract under temperature variations. In the context of the finite element framework that is used to numerically simulate cure-induced damage, the local volume is a single finite element. Therefore and because the crack band method is used, mesh objectivity is included in the formulation.

At the end of step II, the curing process is complete. In step III, the cured RVE (containing cracks or not, as the case maybe) is subjected to transverse tension loading along the 2-direction. The objective here is to compute the strength (S_{22}^{+}) and stiffness (E_{22}) of the virtually cured RVE. Based on the temperature and cure parameters, computation of the stress evolution during cure (step II) and strength calculation based on mechanical loading (step III) is done in a unified step in the commercial software ABAQUS/Standard [18]. In this study, it is assumed that cracking in the curing matrix can occur only for $\phi > 0.2$ and only under tensile stresses.

The crack band model of Bažant and Oh [19] is used to model failure in the matrix. This model assumes that once the critical fracture stress $\sigma_{\rm cr}$ has been reached, microcracks are formed and the additional opening due to cracking is smeared over a band of material. Here the width of that band is taken to be that which lies within an element and perpendicualr to the crack plane. The maximum principal stress criterion is used to determine the failure initiation. In the post-peak regime, the traction-separation law controls the behavior of the damaging material as shown in Figure 1 and the stiffness of the material (matrix) is reduced using the secant value. In the present investigation, $\sigma_{\rm cr}$ is assumed to be independent of ϕ. However, in reality, it is expected that the strength would vary with ϕ. Under mode I cracking, the energy dissipated during the fracturing process is the critical mode I energy release rate ($G_{\rm IC}$) given by

$$G_{\rm IC} = \int_0^{\delta_f} \sigma_{11}(\delta) d\delta = h \int_0^{\varepsilon_f} \sigma_{11}(\varepsilon_{11}) d\varepsilon \tag{8}$$

where stress σ_{11} and ε_{11} are the maximum principal stress and strain values, respectively, and the maximum separation $\delta_f = h\varepsilon_f$ where ε_f corresponds to the critical failure strain of the material (accompanied by complete loss of stiffness). Here, h is the characteristic element length that preserves *mesh objectivity* (see [20]), defined by prescribing a normalized value of $G_{\rm IC}$ for each element such that $g_{\rm IC} = \dfrac{G_{\rm IC}}{h}$. Consequently, the value of $g_{\rm IC}$

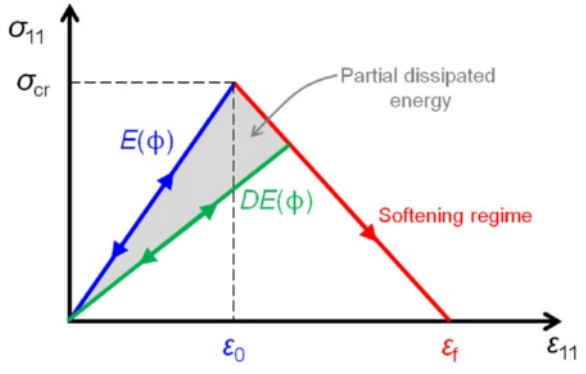

Figure 1 Crack band law in terms of maximum principal stress σ_{11} and maximum principal strain ε_{11}.

equals the area under the $\sigma_{11} - \varepsilon_{11}$ law shown in Figure 1. The value of G_{IC} is chosen to be 0.6 N/mm in all the computations. For a given epoxy system, the values of G_{IC} and σ_{cr} have to be obtained from an experiment, each as a function of the degree of cure ϕ.

From the crack band model formulation, the stiffness reduction factor D with ($0 \leq D \leq 1$) for a material with initial stiffness $E = E(\phi)$ which is now in the softening region of the traction-separation law is computed as

$$D = \frac{\sigma_{\mathrm{cr}}}{E(\varepsilon_f - \varepsilon_{\mathrm{cr}})}\left(\frac{\varepsilon_f}{\varepsilon_{11}} - 1\right) \tag{9}$$

where ε_{11} is the current maximum principal strain value. Thus, $D = 1$ corresponds to no damage, $0 < D < 1$ corresponds to damage but no two-piece failure, while $D = 0$ would indicate complete failure. This D parameter will be used to quantify the extent of stiffness reduction after cure has been completed (i.e., at the end of step II).

Boundary conditions

During curing and mechanical loading, the RVE is subjected to periodic boundary conditions, in concert with the assumption that the RVE is a small volume within an infinite medium. The use of periodic boundary conditions for fiber-reinforced RVEs can be found in the studies of Gonzalez and Llorca [21] and Xia et al. [22], among others. During the cure process (step II), the RVE boundaries are allowed to contract or expand. The RVE can contract or expand depending on temperature change and can contract due to cure shrinkage.

Consider an arbitrary cuboid RVE in the undeformed configuration having lengths L_1, L_2, and L_3 along the x_1, x_2, and x_3 directions with one corner point placed at the origin $(0, 0, 0)$. Then, the equations corresponding to the 3D periodic boundary conditions are

$$\begin{aligned}
u_1(L_1, x_2, x_3) - u_1(0, x_2, x_3) &= \epsilon_{11} L_1 \\
u_2(L_1, x_2, x_3) - u_2(0, x_2, x_3) &= 2\epsilon_{12} L_1 \\
u_3(L_1, x_2, x_3) - u_3(0, x_2, x_3) &= 2\epsilon_{13} L_1 \\
u_1(x_1, L_2, x_3) - u_1(x_1, 0, x_3) &= 2\epsilon_{21} L_2 \\
u_2(x_1, L_2, x_3) - u_2(x_1, 0, x_3) &= \epsilon_{22} L_2 \\
u_3(x_1, L_2, x_3) - u_3(x_1, 0, x_3) &= 2\epsilon_{23} L_2 \\
u_1(x_1, x_2, L_3) - u_1(x_1, x_2, 0) &= 2\epsilon_{31} L_3 \\
u_2(x_1, x_2, L_3) - u_2(x_1, x_2, 0) &= 2\epsilon_{32} L_3 \\
u_3(x_1, x_2, L_3) - u_3(x_1, x_2, 0) &= \epsilon_{33} L_3
\end{aligned} \tag{10}$$

u_1, u_2, and u_3 are the displacements of the RVE boundary along the x_1, x_2, and x_3 directions, respectively, and ϵ_{ij} are the tensorial strains.

Analysis procedure

In summary, the analysis procedure is divided into three steps as shown in Figure 2.

1. *Step I*: A thermochemical analysis is performed using the cure parameters described earlier. Temperature cycle, the degree of cure, and the cure rate in the matrix are provided. Since the RVE dimensions are on the micron scale, there is little to no variation in the temperature field across the RVE. The temperature

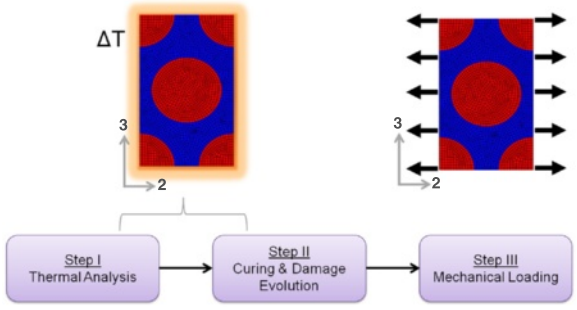

Figure 2 Schematic showing major steps in the analysis. Curing under the prescribed temperature field which includes step I and step II (left). Mechanical loading in the transverse direction to assess the mechanical properties of the virtually cured RVE in step III (right).

profile, the degree of cure (ϕ), and the rate of cure $\left(\frac{d\phi}{dt}\right)$ used in the present study are shown in Figure 3.

2. *Step II*: The stress evolution calculations are preformed as described in Equation 5. Shrinkage during cure is modeled using Equation 7. At the end of this step, we have a virtually cured solid. Possibility of damage during curing is taken into account

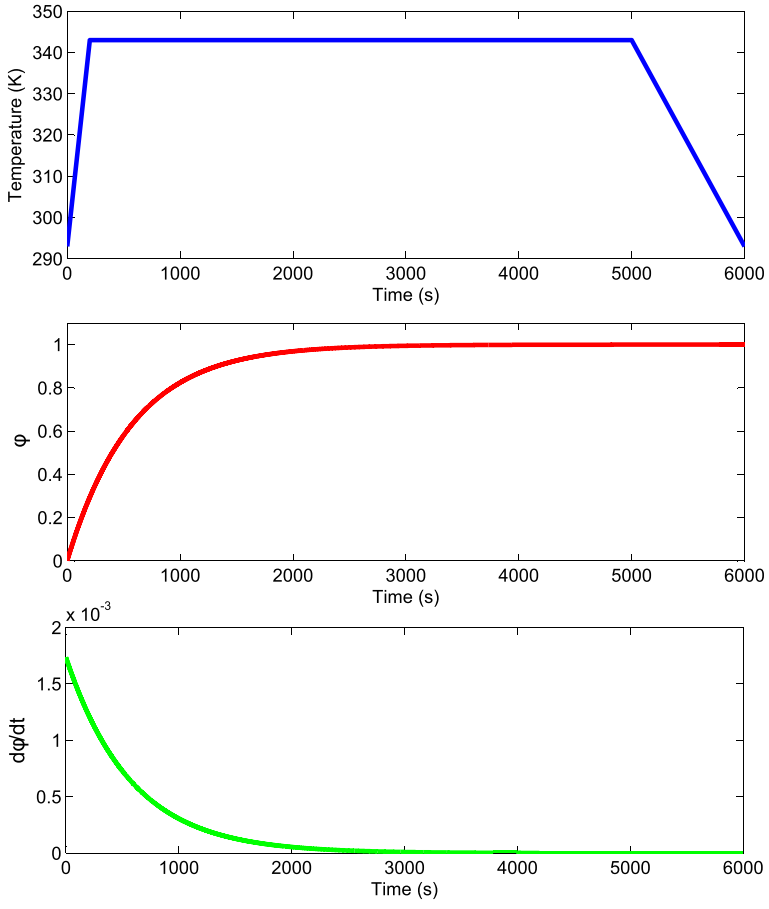

Figure 3 Temperature profile (top), degree of cure ϕ (middle), and rate of cure $\frac{d\phi}{dt}$ (bottom) as functions of time.

using a crack band model. Periodic boundary conditions are enforced throughout this step.

3. *Step III*: The virtually cured RVE is subjected to transverse tensile loading (with periodic boundary conditions in place) to back out the stiffness and strength. Again, the crack band model is used to simulate tensile failure, and periodic boundary conditions are enforced during this step.

Results and discussion

Hexagonally packed fiber RVEs

Three 3D hexagonally packed RVEs with fiber volume fractions (V_f) of 0.5, 0.6, and 0.7 are studied. These RVEs are first subjected to the curing cycle (steps I and II) and then to tensile loading (step III) in the transverse direction. The latter step leads to the determination of the transverse stiffness E_{22} and tensile strength S_{22}^{+} of the virtually cured RVEs. The analysis is done using the finite element software ABAQUS/Standard. The stress evolution expression along with the crack band model is implemented using ABAQUS/Standard's user subroutine UMAT. In each of the RVEs shown in Figure 4, the thickness t along the fiber direction is chosen to be 0.30 μm and carbon fibers are 6 μm in diameter. Both the fiber and the matrix are modeled as isotropic solids. Young's modulus and Poisson's ratio of the fibers are taken to be 200 MPa and 0.3, respectively.

For each of the RVEs shown in Figure 4, three critical fracture strength values (σ_{cr}) of 20, 30, and 45 MPa are chosen which are independent of the degree of cure ϕ, while the critical mode I energy release rate G_{IC} is chosen to be 0.6 N/mm. The strength and toughness are assumed here to be independent of the degree of cure (ϕ). The objective of this portion of the study is to understand how the strength and stiffness of the cured product change with changes in fiber volume fraction and changes in the imposed critical fracture strength during cure. For a given RVE in step II, the matrix tensile stresses can exceed σ_{cr} and microcracks appear leading to a reduction in stiffness. To assess the amount of cure-induced damage, we can keep track of the stiffness reduction factor D at various times during the curing process. Figure 5 shows the average D value for each of the RVEs undergoing cure. Recall that $D = 1$ corresponds to no loss of instantaneous stiffness, whereas $D = 0$ corresponds to the complete loss of stiffness. Here, for each of the RVEs, the D values drop first for the case with $\sigma_{cr} = 20$ MPa followed by the case with $\sigma_{cr} = 30$ MPa and lastly by the case with $\sigma_{cr} = 45$ MPa. This is expected as damage would occur first in the RVE that has the lowest critical strength. Consequently, the RVEs

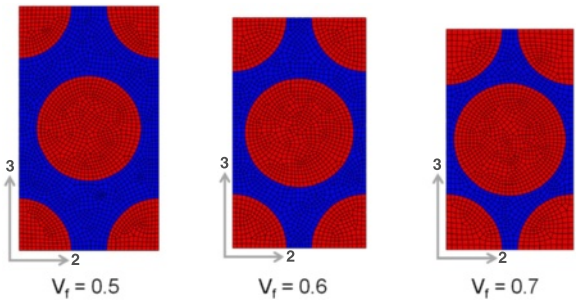

Figure 4 Hexagonally packed fiber-matrix RVEs with fiber volume fractions of 0.5, 0.6, and 0.7. Notice that the dimensions of the fiber are held fixed across these three RVEs.

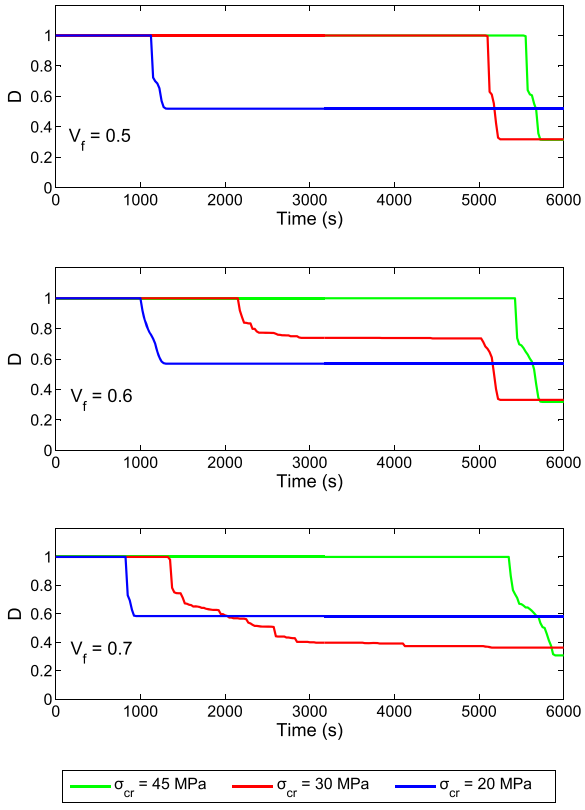

Figure 5 Plots of 'average' stiffness reduction factor D for virtually cured hexagonally packed RVEs during the cure cycle.

with $\sigma_{\text{cr}} = 20$ MPa are also the first to stop curing (locally, at those locations where cracking has occured), on account of microcrack formation. The simulations with σ_{cr} values of 30 and 45 MPa first exhibit microcracks during the cooling phase ($5,000\text{ s} \leq t \leq 6,000\text{ s}$) of the cure cycle where additional shrinkage occurs due to cooling. It is interesting to note that although microcracks appear last for the case with $\sigma_{\text{cr}} = 45$ MPa, the drop in D is more drastic when compared to drops corresponding to the other two cases. Hence, at the end of the cure cycle, for each RVE, the extent of damage varies inversely with the critical fracture strength σ_{cr} of the curing matrix. The spatial variation of D at the end of cure is shown in Figure 6. Even though the RVE is symmetric about a vertical and horizontal line passing through its center, there is nonhomogeneity in the contour of D across the matrix. The nonhomogeneity in D arises because the stress distribution in the RVE does not strictly follow the symmetry present in the hexagonal packing during cure on account of small numerical differences. Hence, once cracking starts at locations where stresses are highest, this breaks the symmetry in stress distribution, thus leading to subsequent nonhomogeneity in D as the curing progresses. In these curing simulations, two-piece failure (corresponding to $D = 0$) was not observed in the cured matrix.

The virtually cured RVEs are now loaded in tension along the transverse direction in step III. As in the previous step, periodic boundary conditions are enforced. The nominal stress-strain ($\sigma_{22} - \varepsilon_{22}$) response is shown in Figure 7. Each of the cured RVEs exhibits a fairly linear response during the initial stages of loading (up to nominal strain), followed

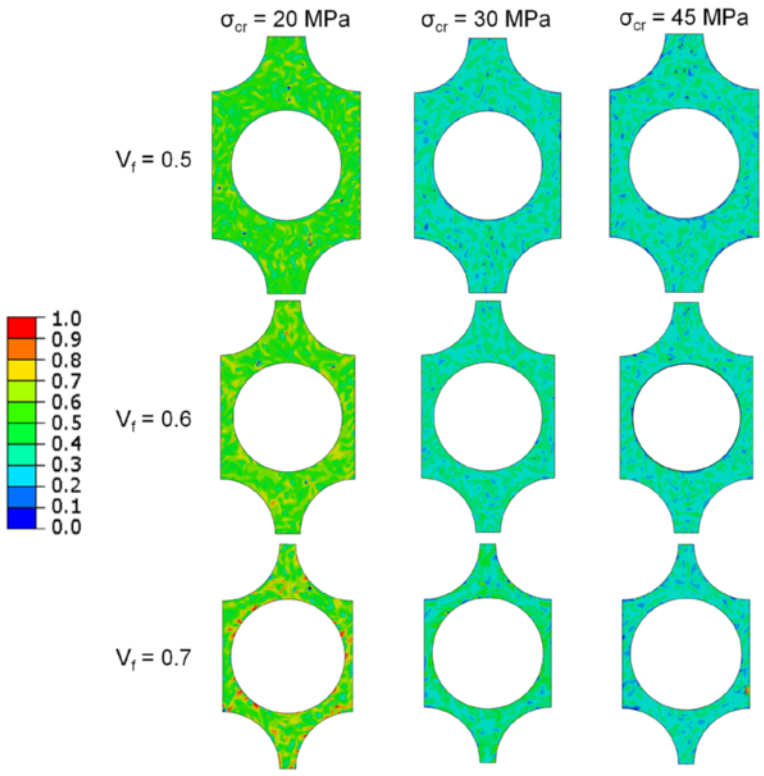

Figure 6 Stiffness reduction factor *D* for the hexagonally packed RVEs at the end of cure.

by a nonlinear softening response before attaining the peak. Past the peak, a rapid drop in stress is observed. The peak stress values correspond to the transverse strength S_{22}^{+} of the virtually cured RVEs. In the case where cure-induced damage is ignored, and when the RVEs are loaded under tension in the transverse direction, the resulting stress-strain response is shown in Figure 8. These RVEs also exhibit a fairly linear response during the initial stages of loading. However, the extent of nonlinearity present before the peak is much lesser than the case when cure-induced damage is accounted for (see Figure 7). The RVEs with no cure-induced damage exhibit higher global stiffness compared to those when cure-induced damage is taken into account. This is as expected. In the post-peak region, the crack paths for simulations with $\sigma_{\mathrm{cr}} = 20$ MPa for virtually cured RVEs and for RVEs where cure-induced damage has not been taken into account are shown in Figure 9 and in Figure 10, respectively. Figure 11 shows the variation of the initial stiffness (E_{22}) of RVEs under mechanical loading. For a given RVE with volume fraction held fixed, the lowest stiffness is exhibited by the RVE having the highest σ_{cr} value of 45 MPa in step II. Recall that from Figure 5, this case with $\sigma_{\mathrm{cr}} = 45$ MPa had the lowest value of D at the end of the cure cycle. Thus, the stiffness reduction factor D is seen to have a positive correlation with global transverse stiffness E_{22} under mechanical loading. Figure 12 shows the comparison of transverse tensile strength S_{22}^{+} values of the virtually cured RVEs and for those RVEs where cure-induced damaged has not been taken into account. It can be seen that for all the volume fractions and all σ_{cr} values considered, the RVEs that have cure-induced damage have noticeably lower strength values.

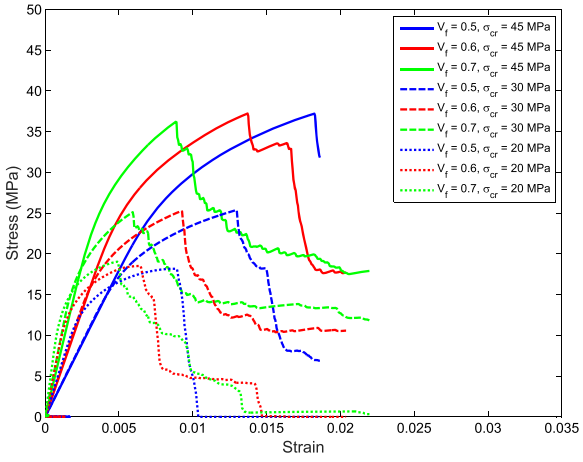

Figure 7 Nominal stress-strain ($\sigma_{22} - \varepsilon_{22}$) response of the hexagonally packed RVEs during step III under transverse tension.

Randomly packed fiber RVEs

Although the RVEs discussed thus far are idealized hexagonally packed geometries, they do not represent a RVE of a realistic FRPC sample. In realistic FRPCs, the fibers are randomly distributed which give rise to several matrix-rich pockets. It would be instructive to understand the severity of the cure-induced damage on the mechanical response, as a function of the randomness in fiber position in an RVE. Eight renditions of square FRPC RVEs with randomly distributed fibers are analyzed in this section. The distribution of fibers within the RVEs was done manually, in that the fibers were arbitrarily placed within the square RVE boundary. The fiber volume fraction (V_f) in all these renditions is chosen to be 0.55. These RVEs are shown in Figure 13. Few strategies to generate random RVEs may be found in the studies of Melro et al. [23], Yang et al. [24], and Vaughan and McCarthy [25]. Recently, using a heuristic random microstructure algorithm, Romanov et al. [26] have generated RVEs that are statistically well correlated with real FRPC RVEs.

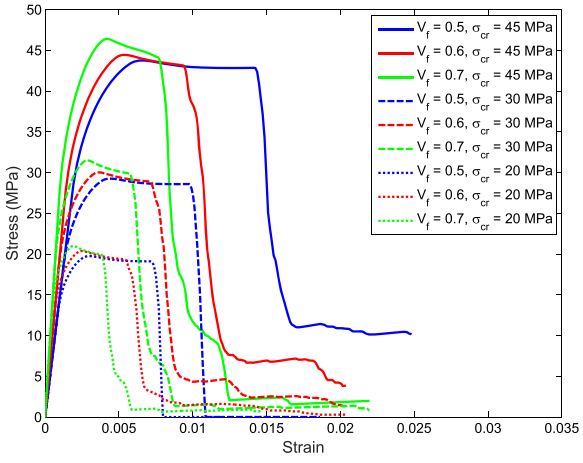

Figure 8 Nominal stress-strain ($\sigma_{22} - \varepsilon_{22}$) response of the hexagonally packed RVEs under transverse tension loading when no damage during cure is assumed.

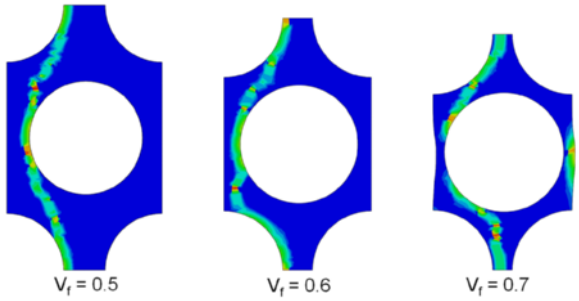

Figure 9 Crack paths under transverse tension loading in hexagonally packed RVEs with $\sigma_{cr} = 20$ MPa.

The cure cycle, fiber, and matrix properties are similar to those used in the aforementioned study with hexagonally packed RVEs. A preliminary analysis on the mesh size has been conducted on a random RVE to establish that important features such as the stiffness reduction factor D at the end of step II and crack path at the end of step III are both mesh insensitive for the range of element sizes analyzed in this study. Figure 14 shows three different levels of refinement for a random packed case study. Results in terms of the factor D and crack path are shown in the top and bottom images of Figure 15, respectively. It can be seen that the spatial distribution of D and the two-piece failure paths are fairly consistent between the three meshes considered, thus establishing mesh objectivity.

Next, the eight random fiber RVEs shown in Figure 13 are cured with the crack band model (with critical fracture stress $\sigma_{cr} = 30$ MPa during cure) prescribed to capture any local matrix damage during cure. Periodic boundary conditions are enforced. The stiffness reduction factor D for these renditions is shown in Figure 16. Each of the RVEs exhibits nonhomogeneity in the contour for D. Note that on account of inherent randomness in fiber packing, there is no symmetry in the RVE at the start of cure. Matrix region areas that are surrounded by closely packed fibers are seen to exhibit higher stresses. This introduces stress gradients in different parts of the RVE during cure. Then, damage initiates at locations where the tensile stresses attain the critical fracture strength σ_{cr}. Therefore, different regions in the virtually cured matrix end up having nonhomogeneous stiffness values owing to different regions damaging differently during cure. These RVEs are next subjected to transverse tension loading along the 2-direction. The nominal stress-strain response is shown in Figure 17. It can be seen that the response is fairly linear during initial stages of loading (for nominal strain $0 \leq \varepsilon \leq 0.0025$). Beyond $\varepsilon > 0.0025$,

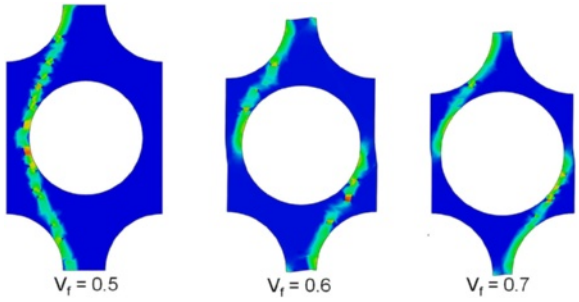

Figure 10 Crack paths under transverse tension loading in hexagonally packed RVEs with $\sigma_{cr} = 20$ MPa, ignoring cure-induced damage.

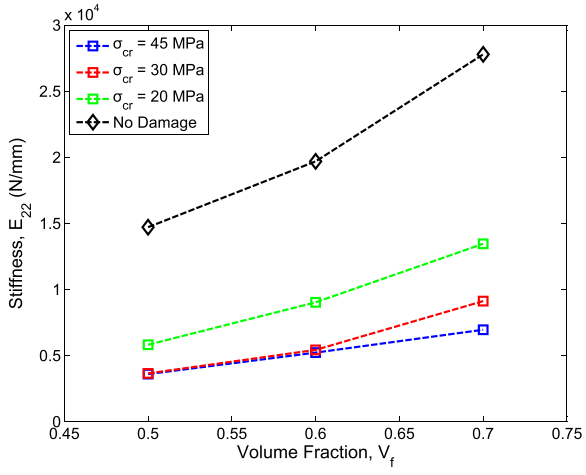

Figure 11 Transverse stiffness E_{22} in hexagonally packed RVEs compared to the case with no cure-induced damage.

there is nonlinear response followed by a peak value between strains of about $\varepsilon \approx 0.008$. Past the peak, the response is like that of a brittle solid, i.e., there is a drastic drop in stress due to two-piece matrix tensile failure. The two-piece crack paths for each of the random RVEs are shown in Figure 18. In some of the RVEs, the crack path is more tortuous than others. It is interesting to look at RVE #5, where there is a prominent and continuous *matrix-rich region* transverse to the loading direction. The two-piece crack path in this RVE at the end of step III is seen to propagate along a zone that has fibers that are more closely packed, which is away from the matrix-rich region. Similar observation holds for RVEs #1, #7, and #9 which have prominent but isolated matrix-rich regions. The matrix which is in a region where fibers are closely packed encounters higher stresses during curing as well as during mechanical loading and is more susceptible to cracking. Thus, cracks tend to initiate and propagate from such sites. The global stress-strain response of the random RVEs when cure-induced damage is not considered is shown in Figure 19.

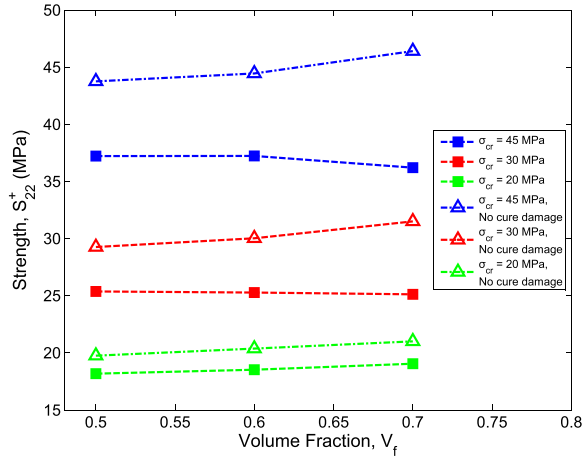

Figure 12 Transverse tensile strength S_{22}^{+} in hexagonally packed RVEs: with and without cure-induced damage.

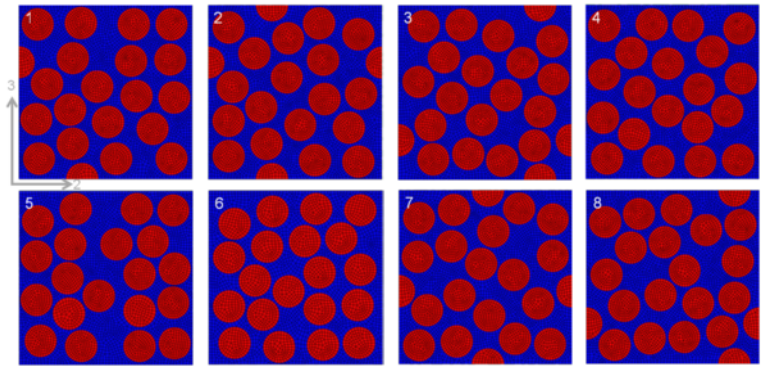

Figure 13 Eight renditions of random 20-fiber RVEs with volume fraction $V_f = 0.55$.

Here, the initial region is fairly linear (for nominal strain $0 \leq \varepsilon \leq 0.002$). However, the stiffness values in the initial region are identical compared to the RVEs with cure-induced damage, where there is a larger spread of the initial stiffness value owing to nonuniform stiffness distribution in the damaged matrix. There is some nonlinearity in the response which is much lesser than that seen in the RVEs when cure-induced damage was considered. A peak is attained beyond which the stress value plateaus momentarily followed by a drastic drop in stress. Finally, the strength values of the two cases (*with* and *without* cure-induced damage) are shown in Figure 20. For each of the RVEs with no cure-induced damage, the transverse tensile strengths are higher, i.e., mean $S_{22}^{+} = 31.2$ MPa compared to mean $S_{22}^{+} = 25.75$ MPa for RVEs with cure-induced damage. Moreover, the scatter in strength values in the RVEs with cure-induced damage is much larger than when no cure-induced damage is taken into account.

In the foregoing sections, we have established that damage in the matrix during cure results in a lower transverse strength value in the virtually cured hexagonally packed RVEs as well as virtually cured randomly packed RVEs. Thus, a comparison of the transverse tensile responses of these two types of RVEs is in order. In hexagonally packed RVEs having a fixed value of critical tensile fracture stress σ_{cr}, the transverse strength S_{22}^{+} did not seem to vary with volume fractions ranging between 0.5 and 0.7 (see Figure 12). However, in randomly packed RVEs, the S_{22}^{+} values exhibited significant scatter (see Figure 20). When compared to the case with no damage during cure, the mean transverse tensile strength reduction for hexagonally packed RVEs (15% reduction) and that for randomly packed RVEs (17% reduction) are similar. The worst strength reduction in randomly packed RVE is 25% for RVE #8. This shows that fiber packing within an RVE has an effect on the strength of the cured RVE with volume fraction held fixed. The effect of

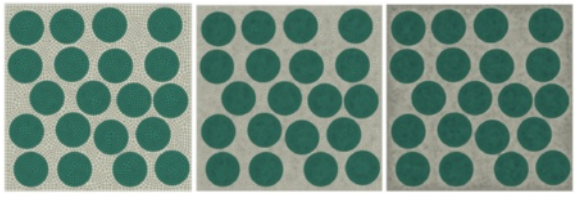

Figure 14 Three mesh sizes chosen for the mesh convergence study.

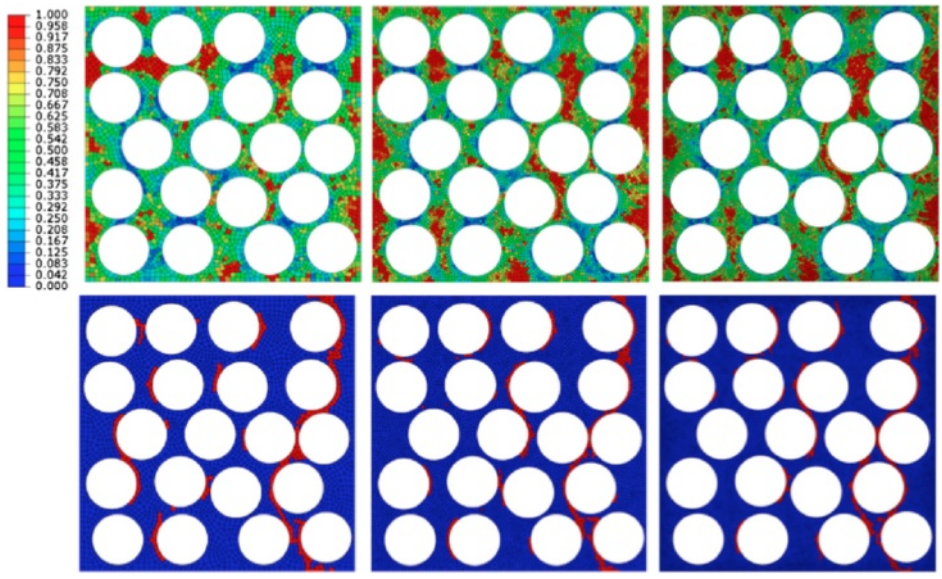

Figure 15 Stiffness reduction factor *D* at the end of cure (top) and crack path (bottom) for three mesh sizes.

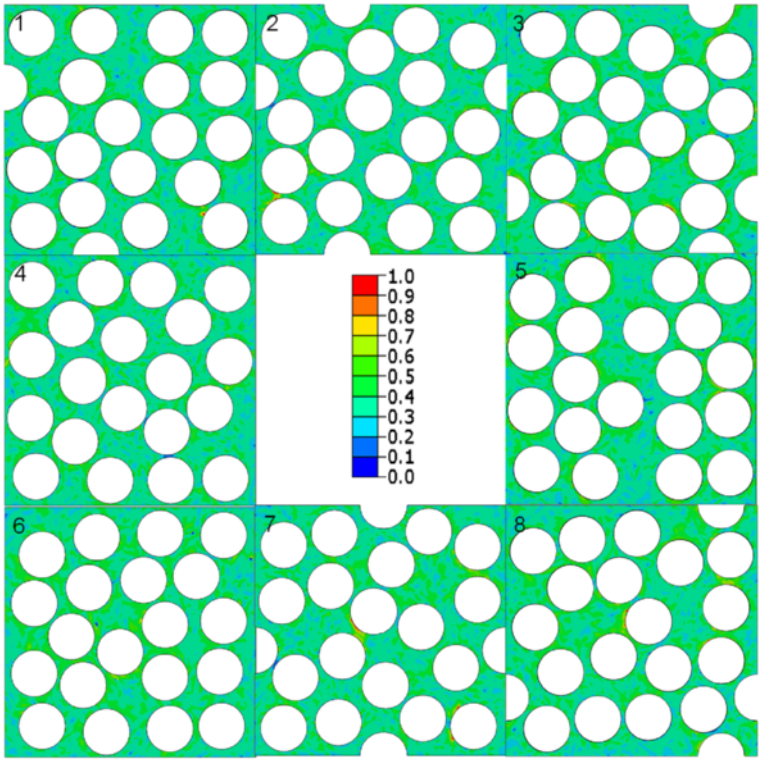

Figure 16 Stiffness reduction factor *D* in the random fiber RVEs at the end of cure.

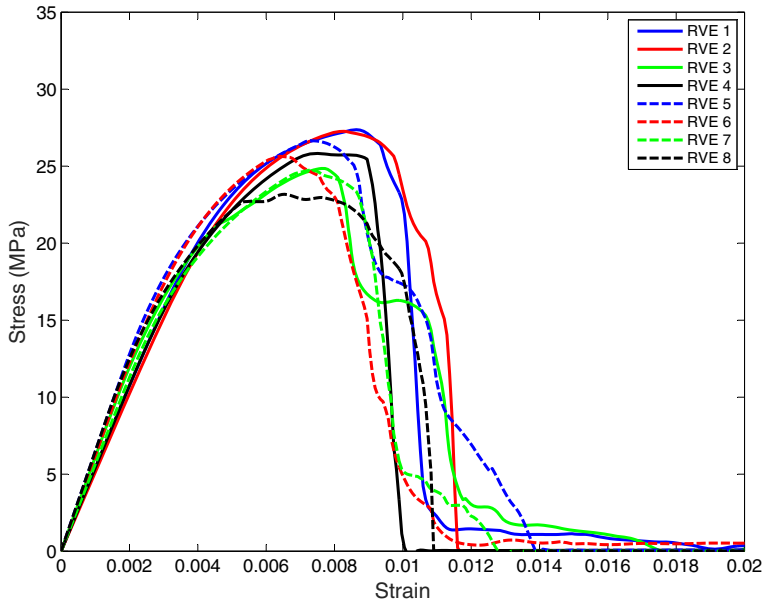

Figure 17 Nominal stress-strain ($\sigma_{22} - \varepsilon_{22}$) response of virtually cured random fiber RVEs having cure-induced damage.

microstructural randomness on mechanical response is detailed in the monograph by Ostoja-Starzewski [27].

Conclusions

The influence of cure on the mechanical response of virtually cured fiber-reinforced polymer matrix RVEs has been studied using a previously reported network model proposed by Heinrich et al. [15] in conjunction with the Bažant-Oh crack band model. Transverse tensile strength (S_{22}^{+}) and transverse stiffness (E_{22}) of these virtually cured RVEs were compared with those when no cure-induced damage was taken into account. These two quantities were calculated from the nominal stress-strain response of the virtually cured RVEs subjected to tensile loading along the transverse direction. Damage during cure is seen to reduce both stiffness and strength of the cured RVEs. Moreover, it is seen that even though fiber volume fraction is held fixed, the transverse strength of the virtually

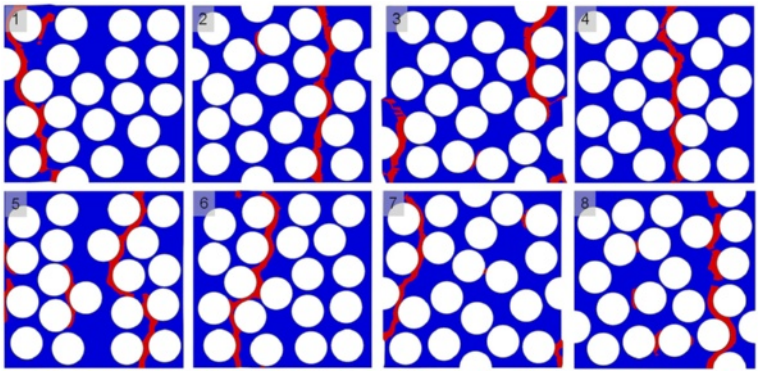

Figure 18 Two-piece crack paths in the randomly packed RVEs under transverse tension loading.

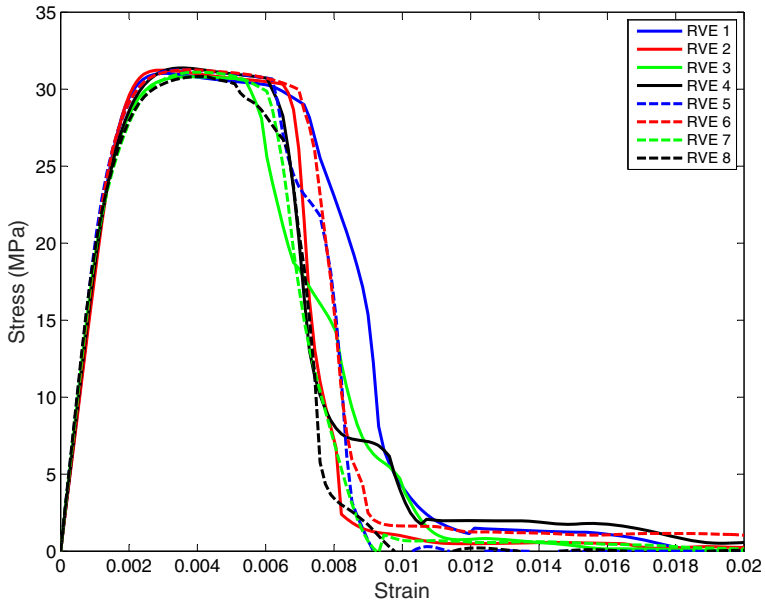

Figure 19 Nominal stress-strain ($\sigma_{22} - \varepsilon_{22}$) response of virtually cured random fiber RVEs with no cure-induced damage.

cured RVEs depend on the fiber packing. Also, the scatter in transverse strength values for RVEs with cure-induced damage is appreciably higher than in the case where cure-induced damage has been neglected. Since fiber packing is seen to influence strength of the cured RVE of constant fiber volume fraction, the study of correlating strength values with some metric associated with fiber packing is delegated to a future study. Using the approach described in this paper, several cure cycles can be considered and eventually tailored to arrive at an optimal cure cycle to reduce damage in the microstructure during the curing process, leading to superior mechanical strength and stiffness of the cured product.

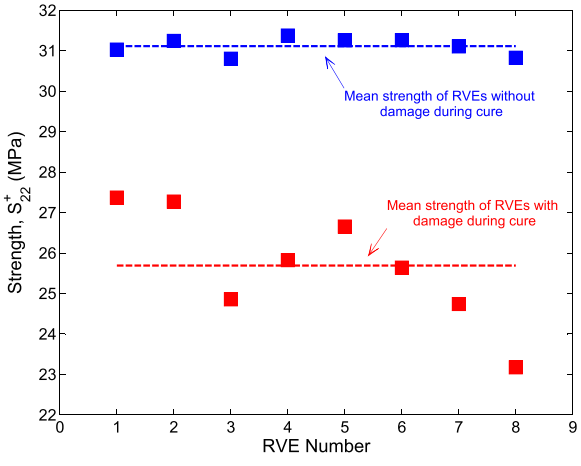

Figure 20 Transverse tensile strength of each random fiber RVE plotted against RVE number.

Competing interests
The authors declare that they have no competing interests.

Authors' contributions
RD and MM conducted the computational analysis and drafted the manuscript. AW conceived the study, its technical foundation, supervised its design and coordination, and contributed to writing the final version. All authors read and approved the final manuscript.

Authors' information
The authors are affiliated with William E. Boeing Department of Aeronautics and Astronautics, University of Washington, Seattle since 1 January 2015.

Acknowledgements
The authors thank Dr. Pascal Meyer and Dr. Christian Heinrich, of the Aerospace Engineering Department at the University of Michigan, Ann Arbor, and Prof. Pavana Prabhakar, Mechanical Engineering Department, University of Texas, El-Paso, for support with the user-defined subroutines used in the present work. The support of the Department of Aerospace Engineering, University of Michigan, Ann Arbor and the William E. Boeing Department of Aeronautics and Astronautics at the University of Washington, Seattle, is gratefully acknowledged.

Received: 8 January 2015 Accepted: 16 March 2015
Published online: 15 April 2015

References
1. Plepys AR, Farris RJ (1990) Evolution of residual stresses in three-dimensionally constrained epoxy resins. Polymer 31(10):1932–1936
2. Plepys AR, Vratsanos MS, Farris RJ (1994) Determination of residual stresses using incremental linear elasticity. Composite Struct 27(1-2):51–56
3. Merzlyakov M, McKenna GB, Simon SL (2006) Cure-induced and thermal stresses in a constrained epoxy resin. Composites: Part A 37:585–591
4. Chekanov YA, Korotkov VN, Rozenberg BA, Dhzavadyan EA, Bogdanova LM (1995) Cure shrinkage defects in epoxy resins. Polymer 36:2013–2017
5. Rabearison N, Jochum C h, Grandidier JC (2009) A FEM coupling model for properties prediction during the curing of any epoxy matrix. Comput Mater Sci 45(3):715–724
6. Ahn J, Waas AM (2002) Prediction of compressive failure in laminated composites at room and elevated temperature. AIAA Journal 40(2):346–358
7. Song S, Waas AM, Shahwan KW, Xiao X, Faruque O (2007) Braided textile composites under compressive loads: modeling the response, strength and degradation. Composite Sci Technol No. 67:3059–3070
8. Kim K, Hahn H (1989) Residual stress development during processing of graphite/epoxy composites. Composites Sci Technol 36:121–132
9. Li M, Zhu Q, Geubelle PH, Tucker III CL (2001) Optimal curing for thermoset matrix composites: thermochemical considerations. Polymer Composites 22:118–131
10. Gopal AK, Adali S, Verijenko VE (2000) Optimal temperature profiles for minimum residual stress in the cure process of polymer composites. Composite Struct 48:99–106
11. White S, Hahn H (1993) Cure cycle optimization for the reduction of processing-induced residual stresses in composite materials. J Composite Mater 27:1352–1378
12. Halpin JC, Kardos JL (1976) Halpin-Tsai equations: a review. Polymer Eng Sci 16(5):344–352
13. Mei Y (2000) Stress evolution in a conductive adhesive during curing and cooling. Ph.D Thesis, University of Michigan
14. Mei Y, Yee AS, Wineman AS, Xiao C (1998) Stress evolution during thermoset cure. Mater Res Soc Symp Proc 515:195–202
15. Heinrich C, Alridge M, Wineman AS, Kieffer J, Waas AM, Shahwan KW (2012) Generation of heat and stress during the cure of polymers used in fiber composites. Int J Eng Sci 53:85–111
16. Kamal MR (1974) Thermoset characterization for moldability analysis. Polymer Eng Sci 14(3):231–239
17. Li C, Potter K, Wisnom MR, Stinger G (2004) In-situ measurement of chemical shrinkage of MY750 epoxy resin by a novel gravimetric method. Composites Sci Technol 64(1):55–64
18. Simulia (2012) Abaqus user manual, version 6.12. Dassault Systèmes, Providence, RI, USA
19. Bažant ZP, Oh B (1983) Crack band theory for fracture of concrete. Mater Struct 16(3):155–177
20. Jirasek M, Bažant ZP (2002) Inelastic analysis of structures. John Wiley & Sons, London and New York
21. Gonzalez C, Llorca J (2007) Mechanical behavior of unidirectional fiber-reinforced polymers under transverse compression: microscopic mechanisms and modeling. Composites Sci Technol 7:2795–2806
22. Xia Z, Zhang Y, Ellyin F (2003) A unified periodical boundary conditions for representative volume elements of composites and applications. Int J Solids Struct 40:1907–1921
23. Melro AR, Camanho PP, Pinho ST (2008) Generation of random distributions of fibers in long-fibre reinforced composites. Composites Sci Technol 68(9):2092–2102
24. Yang L, Ying Y, Ran Z, Liu Y (2013) A new method for generating random fiber distributions for fiber reinforced composites. Composites Sci Technol 76:14–20
25. Vaughan TJ, McCarthy CT (2010) A combined experimental-numerical approach for generating statistically equivalent fiber distributions for high strength laminated composite materials. Composite Sci Technol 70(2):291–297
26. Romanov V, Lomov SV, Swolfs Y, Orlova S, Gorbatikh L, Verpoest I (2013) Statistical analysis of real and simulated fibre arrangements in unidirectional composites. Composite Sci Technol 87:126–134
27. Ostoja-Starzewski M (2007) Microstructural randomness and scaling in mechanics of materials. Chapman and Hall-CRC 2007, Florida, USA